THE JOURNAL OF PHYSICAL CHEMISTRY C

Article

pubs.acs.org/JPCC

Network Analysis of Photovoltaic Energy Conversion

Mario Einax* and Abraham Nitzan*

School of Chemistry, Tel Aviv University, Tel Aviv 69978, Israel

Supporting Information

ABSTRACT: Photovoltaic energy conversion in photovoltaic cells has been analyzed by the detailed balance approach or by thermodynamic arguments. Here we introduce a network representation to analyze the performance of such systems once a suitable kinetic model (represented by a master equation in the space of the different system states) has been constructed. Such network representation allows one to decompose the steady state dynamics into cycles, characterized by their cycle affinities. Both the maximum achievable efficiency and the open-circuit voltage of the device are obtained in the zero affinity limit. This method is applied to analyze a microscopic model for a bulk heterojunction organic solar cell that includes the essential optical and interfacial electronic processes that characterize this system, leading to an explicit expression for the theoretical efficiency limit in such systems. In particular, the deviation from Carnot's efficiency associated with the exciton binding energy is quantified.

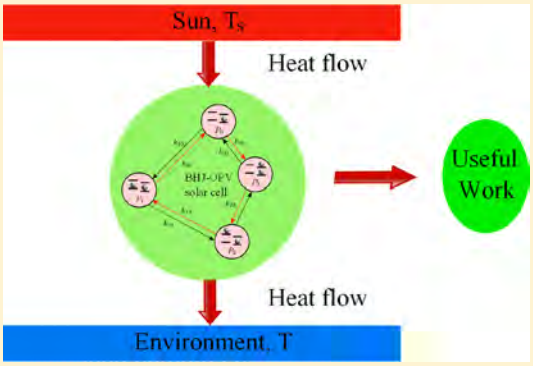

1. INTRODUCTION

The quest to improve the efficiency of solar energy conversion is the focus of intensive current research.[1−3] In particular, considerable attention has focused recently on organic solar cells, where advantageous low manufacturing cost is still counterbalanced by a relatively low energy conversion yield, associated with the fact that light absorption in such low dielectric permittivity materials forms excitons, that is, electron−hole pairs,[4] that require extra energy for dissociation.[5−13]

Such energy conversion studies naturally involve questions concerning efficiency,[11,14−17] in particular the possible existence of fundamental limits on this efficiency.[18−23] Obviously, the efficiency of any individual photovoltaic system intimately depends on its structure, but as much as is done for heat engines, it is of interest to understand it on the generic level which starts with the determination of the maximum efficiency and follows by identifying and analyzing processes that reduce it. The seminal work of Shockley and Queisser (SQ)[18] is a prominent example. In that work, a thermodynamic analysis of semiconductor (SC)-based solar cells is carried out under the assumptions that all photons with energies larger than the SC band gap are absorbed, focusing mostly on losses associated with radiative recombination of electron−hole pairs (an unavoidable process whose existence follows from the principle of detailed balance). With these model assumptions, and using thermodynamic considerations formulated in terms of the detailed balance principle, SQ has provided a simple analysis of the maximal ensuing cell efficiency. Several works[24−28] have extended the SQ analysis to more complex models, e.g., organic photovoltaic (OPV) cells.[13,16,21,22,24,27−29] Others have formulated abstractions of the SQ model (sometimes with generalizations that account for carrier nonradiative recombination) in order to study its kinetics and thermodynamics foundation.[30−35] Recent works have also studied the possible implications of quantum coherence in the quantum analogues of such kinetic models.[36−39]

The overall, so-called *external*, efficiency of a photovoltaic energy conversion system is defined as the ratio between the output converted power and the optical energy per unit time incident on the system. It is a product of the *internal efficiency*—the ratio between the output power and the optical energy absorbed by the system per unit time and the ratio between the incident and absorbed powers. This ratio depends on the spectral structure of incident radiation, the absorption spectrum of the systems, and geometric factors such as the incident angle.[40] The focus of our discussion is the internal efficiency, which is the analogue of the thermodynamic efficiency of a heat engine. Indeed, at the core of many generic approaches to this factor in the performance of photovoltaic cells is the use of thermodynamics to analyze energy exchange and conversion processes in the limit of vanishing current, that is, zero power. Such analysis can provide generic results for maximal efficiencies at the cost of being limited to zero power processes. Consideration of such systems under finite power operation requires more detailed information about the underlying rate processes, and their studies constitute ongoing efforts in the field of finite time thermodynamics (see, e.g., refs 41−57). While applications to photovoltaic systems were done for specific model systems (see, e.g., ref 32), it is of interest to find a general formulation and generic principles that underline the analysis of such situations. The purpose of the present

Received: August 20, 2014
Revised: November 1, 2014
Published: November 3, 2014

   dx.doi.org/10.1021/jp5084373 | J. Phys. Chem. C 2014, 118, 27226−27234

paper is to describe an approach for such a formulation and to demonstrate its utility in some model systems.

Our approach is formulated in the framework of network theory as applied to steady state systems.[58−64] Inspired by the Kirchoff laws,[65] applications of this theory to the performance analysis of chemical reaction networks are well-known in diverse areas such as chemical engineerng[66] and chemical biology,[67] but we are not aware of such work on photovoltaic systems. The starting point is a representation of the system dynamics by a kinetics scheme comprising system states connected by (assumed known) rates, similar in spirit to transport theories based on lattice gas approaches,[68−71] that find applications in other contexts, e.g., use a master equation approach to analyze cell dynamics.[15,24,72,73] In the graph theory approach this kinetic scheme is represented by a graph that comprises nodes (corresponding to states) and edges (representing transitions between states), on which fluxes associated with the nonequilibrium dynamics flow along interconnected linear and cyclical paths. In this scheme, the observed macroscopic currents (average currents of macroscopic variables) through the systems are linked through their circular counterparts to the microscopic transitions between individual states. It has been shown by Schnakenberg[59] that for each cycle an associated entropy production (called affinity of cycle) can be obtained as the ratio between the product of all transition rates in the forward direction and the corresponding product of transition rates in the reversed direction. Then, the upper efficiency limit and the open-circuit voltage of a large class of systems follow straightforwardly by setting the cycle affinity of a basic cycle (that contains the photovoltaic operation of the device) to zero. At the same time, the finite power operation of such systems can be analyzed by addressing the underlying kinetic equation.

When applied (Section 2) to the simplest two-level model of refs 30 and 32, this framework yields a formalism similar to that considered in these papers, with the Carnot efficiency (albeit with an effective "sun temperature" that reflects the presence of nonradiative relaxation and excitation) marking the zero power limit. Given the underlying kinetic equations, it is easy to analyze the finite power operation of this simple generic model, leading to an analytical expression for the maximal power. As expected, in contrast to the zero power limit, the finite power efficiency is not a universal function of the operating effective temperatures but depends on the individual rates. Interestingly we find that, at least for this model, this dependence is quite weak for the internal efficiency but considerable when the external efficiency is considered.

Coming back to the zero power limit, the strength of this graph theory approach becomes apparent when more complex models are analyzed. In Sections 3 and 4 we consider the thermodynamic efficiency limit in the simplest (six-level) kinetic model[33,34] for an organic bulk heterojunction (BHJ) photovoltaic cell. This analysis shows that when the exciton binding energy is non-negligible the molecular heat engines operates with a maximum (zero power) efficiency which is fundamentally lower than the Carnot efficiency. This finding recovers the numerical observation in ref 33 and is compatible with the result obtained from the second law of thermodynamics in ref 21. As expected, in the limit of zero exciton binding energy, the theoretical efficiency limit approaches the universal upper bound given by the Carnot efficiency.

While this six-state BHJ-OPV model is considered in detail, it is made evident that this type of analysis can be applied in far more complex situations. In Section 5 we discuss possible extensions of the present work that will be addressed in future studies.

2. TWO-LEVEL PHOTOVOLTAIC MODEL

As in refs 30, 32, and 74, we consider a photovoltaic device comprising a two-level system situated between two external contacts, L and R (see Figure 1a), so that level 1 is coupled only

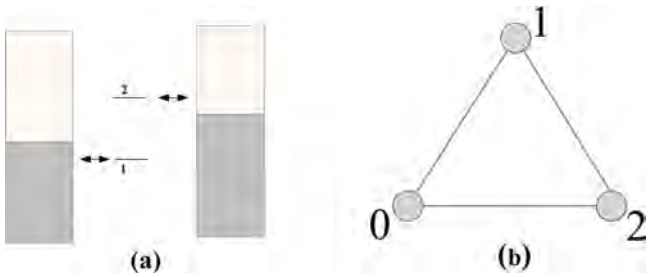

Figure 1. Spinless two-level, three-state model of a solar device that comprises two metal electrodes and a two-level molecule. Levels 1 and 2 are coupled to the left and right electrodes, respectively. The molecule can be in states $0 = |0,0\rangle, 1 = |1,0\rangle$ and $2 = |0,1\rangle$ where $|n_1,n_2\rangle$ is a state with n_1 electrons in level 1 and n_2 electrons in level 2 (double occupancy is not allowed).

to the left electrode while level 2 sees only the right electrode. For simplicity we disregard the electron spin and exclude double occupancy of the two-level system. This device can thus be in three states—0, vacant; 1, electron in level 1; and 2, electron in level 2—that constitute a simple cyclical network (Figure 1b) in which each vertex represents a state and each edge connecting two vortices corresponds to a pair of forward and back rates

$$0 \underset{k_{01}}{\overset{k_{10}}{\rightleftharpoons}} 1 \underset{k_{12}}{\overset{k_{21}}{\rightleftharpoons}} 2 \underset{k_{20}}{\overset{k_{02}}{\rightleftharpoons}} 0 \tag{1}$$

Under conditions that lead to equilibrium at long time, the ratios between these rates are determined by the ambient temperature T, the level energies E_1, E_2, and the chemical potential μ that characterizes electrons in the metal electrodes and are given by the detailed balance relations

$$\frac{k_{10}}{k_{01}} = e^{-\beta(E_1-\mu)}; \quad \frac{k_{21}}{k_{12}} = e^{-\beta(E_2-E_1)}; \quad \frac{k_{20}}{k_{02}} = e^{-\beta(E_2-\mu)} \tag{2}$$

where $\beta = 1/k_BT$ is the inverse thermal energy and k_B is the Boltzmann constant. Note that the rates k_{21} and k_{12} can originate from radiative transitions (thermal radiation) as well as nonradiative processes, both characterized by the ambient temperature T. At equilibrium all fluxes vanish, $J_{ji} = k_{ji}P_i^{eq} - k_{ij}P_j^{eq} = 0$, where P_j is the probability that the system is in state j. A cyclical network of this property is characterized by the identity

$$\frac{k_{02}k_{21}k_{10}}{k_{20}k_{12}k_{01}} = 1 \tag{3}$$

that is satisfied by the ratio between forward and backward rates in a reaction loop, provided that these rates sustain a state of zero loop current.

In an operating photovoltaic cell the system is taken out of this equilibrium in two ways: (a) Radiative pumping (and

dx.doi.org/10.1021/jp5084373 | J. Phys. Chem. C 2014, 118, 27226−27234

damping) is affected on the 1−2 transition. In standard models of photovoltaic cells this pumping is represented by an effective temperature $T_s = 1/k_B\beta_s$ ("sun temperature"[75]). With the coupling scheme (eq 1), this leads to electron current from the left to the right electrode; however, this *short-circuit current* does not perform any useful work unless (b) an opposing voltage bias $U = \Delta\mu/e$ is set between the two electrodes ($\Delta\mu$ is the corresponding chemical potential difference) so that the photocurrent works against this bias. The kinetic rates now satisfy

$$\frac{k_{10}}{k_{01}} = e^{-\beta(E_1-\mu_1)}; \quad \frac{k_{21}}{k_{12}} = e^{-\beta_s(E_2-E_1)}; \quad \frac{k_{20}}{k_{02}} = e^{-\beta(E_2-\mu_2)} \tag{4}$$

where $\mu_2 = \mu_1 + \Delta\mu$ and $T = 1/k_B\beta$ is the ambient temperature. At steady state, the current J is the same on all segments of the graph of Figure 1b

$$J = k_{10}P_0 - k_{01}P_1 = k_{21}P_1 - k_{12}P_2 = k_{02}P_2 - k_{20}P_0 \tag{5}$$

The *open-circuit* (OC) *voltage* is the bias for which this current vanishes. The existence of such a state again implies that these rates satisfy eq 3. Equations 3 and 4 then lead to

$$\eta^{OC} \equiv \frac{\Delta\mu^{OC}}{E_2 - E_1} = 1 - \frac{T}{T_s} \tag{6}$$

Viewed as the zero current limit of the (thermodynamic or internal) efficiency $J\Delta\mu/[J(E_2 - E_1)]$ (ratio between the work per unit time, $\dot{W} = J\Delta\mu$, extracted from the device and the heat per unit time, $\dot{Q}_S = (E_2 - E_1)J$, absorbed from sun), eq 6 simply identifies the efficiency in this reversible (zero current) limit as the Carnot efficiency. Remarkably, this result does not depend on the relative alignment of the molecular levels with respect to the electrode Fermi levels. It does rely on the assumption that all input "sun heat" enters at the resonance energy $E_2 - E_1$ and identifies the inability of this system to efficiently extract energy from photons of different energies as an important source of loss.

The advantage of using such cycle analysis is that it is easily generalizable to any model that can be represented by a network of states and rates. As a prelude to the model of organic photovoltaic cells considered in the following sections, we note that the three-state model used above relies on the assumption that the system cannot be doubly occupied. Removing this restriction yields the slightly more complex model of Figure 2 that can be analyzed in the same way. It is

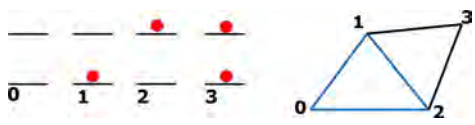

Figure 2. Two-state model with double occupation allowed.

immediately seen that the condition of zero current, that is, the vanishing of fluxes on the 0−1, 0−2, 1−3, and 2−3 bonds, implies that current must be zero also on the 1−2 bond. It can therefore be asserted without an additional calculation that the result 6 for the open-circuit voltage holds also for this extended model.

Once a kinetic model such as given by eqs 1 and 4 has been defined, it is also possible to evaluate its dynamical properties. Of particular interest in the present context is the optimal efficiency at finite power. While a general discussion of this issue will be the subject of a separate publication, we provide below and in the Supporting Information an outline of such calculation for the present two-level/three-state model. First and foremost, it is important to realize that unlike in equilibrium the finite power performance is not a universal function of the external driving parameters (voltage, effective temperatures, light intensity, etc.) but depends on details of internal system rates and on the way the system is taken out of equilibrium. As a specific example we start from an open-circuit situation, in which the kinetic rates satisfy eq 4 with given OC potentials $\mu_j = \mu_j^{OC}$, j = 1,2, and OC bias $\Delta\mu^{OC} = \mu_2^{OC} - \mu_1^{OC}$. The corresponding population probabilities $P_k = P_k^{OC}$ and k = 0,1,2 are obtained from eq 5 with $J = 0$ to be

$$P_0^{OC} = \frac{1}{1 + e^{-\beta(E_1-\mu_1)} + e^{-\beta_s(E_2-E_1)}e^{-\beta(E_1-\mu_1)}} \tag{7}$$

$$P_1^{OC} = \frac{1}{1 + e^{\beta(E_1-\mu_1)} + e^{-\beta_s(E_2-E_1)}} \tag{8}$$

$$P_2^{OC} = \frac{1}{1 + e^{\beta_s(E_2-E_1)} + e^{\beta_s(E_2-E_1)}e^{\beta(E_1-\mu_1)}} \tag{9}$$

As pointed out, the system performance away from the OC situation depends on details of the kinetic rates. Below we focus on the following choice for the OC rates

$$k_{01} = \nu_1(1 - f(x_1)); \quad k_{10} = \nu_1 f(x_1);$$
$$k_{02} = \nu_2(1 - f(x_2)); \quad k_{20} = \nu_2 f(x_2) \tag{10}$$

$$k_{12} = \nu_s(1 + n(x_s)); \quad k_{21} = \nu_s n(x_s) \tag{11}$$

where $f(x)$ and $n(x)$ are Fermi−Dirac and Bose−Einstein distributions, respectively

$$f(x) = (e^x + 1)^{-1}; \quad n(x) = (e^x - 1)^{-1} \tag{12}$$

and where

$$x_k = \beta(E_k - \mu_k); \quad k = 1, 2; \quad x_s = \beta_s(E_2 - E_1) \tag{13}$$

Furthermore, finite power operation is induced by changing the electrochemical potential on electrode 2

$$\mu_2 = \mu_2^{OC} - \Delta\mu_2 \text{ so that } \Delta\mu = \Delta\mu^{OC} - \Delta\mu_2 \tag{14}$$

keeping all other system parameters and driving forces fixed. Obviously, in eq 4 only k_{02}, k_{20} are affected

$$\frac{k_{20}}{k_{02}} = e^{-\beta(E_2-\mu_2^{OC})} \Rightarrow \frac{k_{20} + \delta k_{20}}{k_{02} + \delta k_{02}} = e^{-\beta(E_2-\mu_2^{OC}+\Delta\mu_2)} \tag{15}$$

However, the calculated efficiency at maximum power will depend on the particular choice of δk_{20} and δk_{02}. Below we show results for the choices

Case (a)

$$\delta k_{02} = 0, \quad \delta k_{20} = k_{20}^{OC}(e^{-\beta\Delta\mu_2} - 1) \tag{16a}$$

Case (b)

$$\delta k_{20} = 0, \delta k_{02} = k_{02}^{OC}(e^{\beta\Delta\mu_2} - 1) \tag{16b}$$

Once the new rates are given, here by eqs 15 and 16, eq 5 together with the probability normalization condition can be solved to yield the steady state current $J(\Delta\mu) = J(\Delta\mu^{OC} - \Delta\mu_2)$ in terms of the potential $\Delta\mu_2$ that carries the system outside the OC situation. This function can be inverted to yield the bias

dx.doi.org/10.1021/jp5084373 | J. Phys. Chem. C 2014, 118, 27226−27234

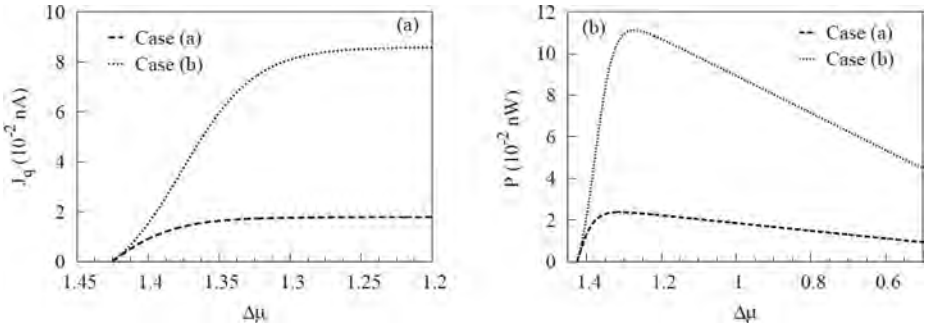

Figure 3. Steady state electrical current $J_q = eJ$ with e = electron charge (a) and power, $J\Delta\mu$ (b), delivered by a system described by the two-level/three-state model of Section 3, displayed as functions of the imposed bias, $\Delta\mu = \Delta\mu^{OC} - \Delta\mu_2$. For the system parameters used (given in the text) the open-circuit voltage is $\Delta\mu^{OC} = 1.425$ eV. The bias is varied by changing the potential on electrode 2, $\mu_2 = \mu_2^{OC} - \Delta\mu_2$, and results are displayed for two different ways (a) and (b) (defined by eq 16) by which the system is taken away from the OC situation.

$\Delta\mu(J)$ needed to maintain a steady current J. The delivered power is $P = J\Delta\mu$, and the corresponding efficiency is

$$\eta(J) \equiv \frac{P}{J(E_2 - E_1)} = \frac{\Delta\mu(J)}{E_2 - E_1} \tag{17}$$

Finally, for the model addressed here, the bias for optimal (maximum delivered power) operation is $\Delta\mu^* = \Delta\mu^{OC} - \Delta\mu_2^*$ where $\Delta\mu_2^*$ is obtained from the equation

$$\frac{dP}{d(\Delta\mu_2)} = -J(\Delta\mu^{OC} - \Delta\mu_2) + (\Delta\mu^{OC} - \Delta\mu_2)\frac{dJ(\Delta\mu^{OC} - \Delta\mu_2)}{d(\Delta\mu_2)} = 0 \tag{18}$$

Further technical details are given in the Supporting Information. Figures 3 and 4 show results of this calculation

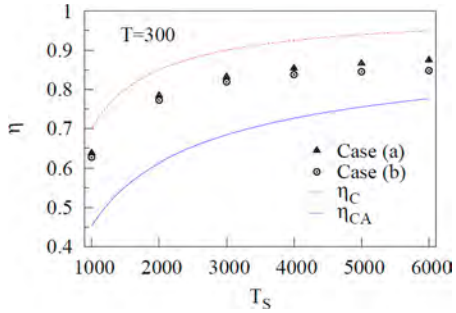

Figure 4. Thermodynamic efficiencies at maximum power of the two-level/three-state model with the choice of parameters and rates given in the text, displayed as functions of the higher ("sun") temperature T_S with the ambient temperature $T = 300$ K for cases (a) and (b) of eq 16. Also shown are the Carnot upper bound ($\eta_C = 1 - T/T_S$) and the Curzon-Ahlborn effciency $\eta_{CA} = 1 - (T/T_S)^{1/2}$.

for a particular choice of parameters, $E_1 = -0.1$ eV, $E_2 = 1.4$ eV, $\mu_1 = 0.0$ eV, $T = 300$ K, $T_s = 6000$ K, and $\nu_1 = \nu_2 = \nu_S = 1 \times 10^{-10}$ s^{-1}. Shown are the steady state current (Figure 3a) and power (Figure 3b) as a function of the imposed bias when μ_2 is changed from its OC value, as indicated by eq 14. For this choice the open-circuit voltage (from eq 6) is $\Delta\mu^{OC} = \mu_2^{OC} = 1.425$ eV, and the Carnot efficiency is 0.95. For the optimal finite power operation, the solution of eq 18 yields $\Delta\mu_2^* = 0.113$ eV and $\eta(\Delta\mu_2^*) = 0.874$ for case (a) and $\Delta\mu_2^* = 0.153$ eV and $\eta(\Delta\mu_2^*) = 0.848$ for case (b). For this choice of parameters and for cases (a) and (b) the short-circuit currents J_q^{SC} are 1.776 and 8.579 nA; the maximal delivered powers are $P^* = 2.376$ and 11.121 nW; and the corresponding filling factors are $f = P^*/(\Delta\mu^{OC}J_q^{SC}) = 0.903$ and 0.875, respectively.

Figure 4 displays the efficiency at maximum power of the present model as a function of the higher ("sun") temperature in comparison to the Carnot and the Curzon-Ahlborn[76] (CA; $\eta_{CA} = 1 - (T/T_S)^{1/2}$) efficiencies. Previous work has indicated that the latter provides a good approximation to the effciency at maximum power of the present model. As argued above, the efficiency at maximum power is not a universal function of the operating temperatures, and Figure 4 shows that with our choices of kinetic parameters the effciency can appreciably exceed the CA result.

The above results are most easily interpreted in the absence of nonradiative $1 \rightleftharpoons 2$ relaxation. In general such relaxation does take place so that

$$k_{12} = k_{12}^R + k_{12}^{NR}; \quad k_{21} = k_{21}^R + k_{21}^{NR} \tag{19}$$

where the superscripts R and NR denote radiative and nonradiative processes, respectively. While the radiative rates satisfy a detailed balance (e.g., eq 11) at the sun temperature, the ratio between the upward and downward nonradiative rates corresponds to the ambient temperature. The radiative rates are photoinduced by sunlight and satisfy a detailed balance condition associated with the sun temperature T_s, while the nonradiative rates are determined by interaction with the environment and obey a detailed balance relation governed bythe ambient temperature

$$\frac{k_{21}^R}{k_{12}^R} = e^{-(E_2-E_1)/k_BT_S}; \quad \frac{k_{21}^{NR}}{k_{12}^{NR}} = e^{-(E_2-E_1)/k_BT} \tag{20}$$

Obviously, an effective temperature can be defined from

$$\frac{k_{21}}{k_{12}} = e^{-\beta_{eff}(E_2-E_1)}; \quad \beta_{eff} = (k_BT_{eff})^{-1} \tag{21}$$

and all the results above are obtained with T_s replaced by T_{eff}. In particular the open-circuit efficiency given by eq 6 will be smaller in the presence of nonradiative relaxation because $T_{eff} < T_S$. It should be noted however that the internal efficiency was defined here (eq 17) as the ratio between the delivered power and the input power where the latter was defined in terms of the total net current J as $J(E_2 - E_1)$. Another common practice[32,33] is to define the input power as $J_s(E_2 - E_1)$ where J_s is the current associated with the sun-induced process only, $J_s = k_{21}^R P_1 - k_{12}^R P_2 = J - (k_{21}^{NR}P_1 - k_{12}^{NR}P_2) \cong J + k_{12}^{NR}P_2$. Denoting the efficiency defined in this way by η_s we obtain

dx.doi.org/10.1021/jp5084373 | J. Phys. Chem. C 2014, 118, 27226−27234

$$\eta_s = J\Delta\mu(J)/J_s(E_2 - E_1) = \eta\frac{J}{J_s} \quad (22)$$

Obviously $\eta_s \leq \eta$, where the equality holds in the absence of nonradiative relaxation. In particular, in the OC limit, when η becomes the Carnot efficiency $1 - T/T_{eff}$ associated with the effective temperature defined by eq 21, η_s vanishes since $J = 0$ in this limit.

Finally, we note the efficiency addressed above in the thermodynamic "internal" efficiency. More relevant to assessment of solar cell operation is the external efficiency that relates the useful output power to the total power incident on (but not necessarily absorbed by) the systems. The results shown above indicate that while internal efficiency at maximum power depends on details of the kinetic rates that characterize the system as well as the way the external load is applied this dependence is rather weak. In contrast, the maximal external efficiency, which is simply proportional to the maximum power delivered by the system, is seen (Figure 3b) to be highly sensitive to these details.

This simple example demonstrates the use of kinetic schemes that incorporate rate information in the analysis of photovoltaic device performance, as well as its relationship to thermodynamics. Naturally, Carnot efficiency is realized in the OC limit. In the following two sections we apply a similar analysis to a simple model of bulk heterojunction organic photovoltaic (BHJ-OPV) cells, where essential internal losses lead to a maximum (internal) efficiency that is lower than the Carnot result.

3. BHJ-OPV MODEL

The BHJ-OPV cell model considered here is comprised of two effective sites l = D, A representing the donor (D) and the acceptor (A) molecules, in contact with two electrodes, L and R (see Figure 5). Each of the sites is described as a two-state

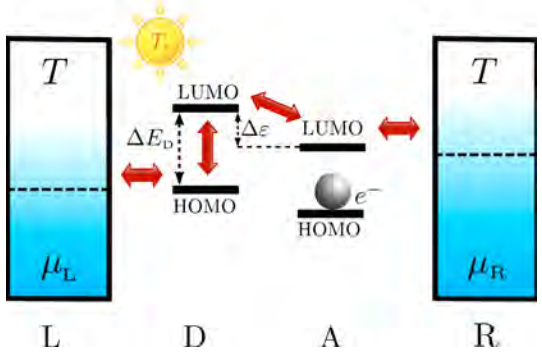

Figure 5. Schematic representation of energetics in BHJ solar cells. The system consists of a donor and acceptor, each characterized by their HOMO and LUMO levels.

system with energy levels (ε_{D1},ε_{D2}) and (ε_{A1},ε_{A2}) corresponding to the highest occupied and lowest unoccupied molecular orbital (HOMO, LUMO) levels of the donor and acceptor species, respectively. The electrodes are represented by free-electron reservoirs at chemical potentials μ_K (K = L,R) that are set to $\varepsilon_F = \varepsilon_{D1} + \Delta E_D/2$ ($\Delta E_D = \varepsilon_{D2} - \varepsilon_{D1}$) in the zero-bias junction. The electrochemical potential difference corresponds to a bias voltage $U = (\mu_R - \mu_L)/|e|$, where $|e|$ is the electron charge. In what follows we use the notation $\Delta E_l = \varepsilon_{l2} - \varepsilon_{l1}$ (l = D,A) for the energy differences that represent the donor and acceptor band gaps and refer to $\Delta\varepsilon = \varepsilon_{D2} - \varepsilon_{A2}$ as the interface or donor−acceptor LUMO−LUMO gap.[77] The different system states are described by occupation numbers n_{Kj} = 0,1, where K = D,A and j = 1,2.

To further assign realistic contents to this model we introduce the restrictions $n_{D1}n_{D2} = 0$ (i.e., the donor cannot be double occupied) and $n_{A1} = 1$. The second condition implies that the acceptor can only receive (and subsequently release) an additional electron. Because of this restriction, the energy ε_{A2} can be taken as the corresponding single electron energy given that level A1 is occupied. The resulting microscopic description then consists of six states with respect to the occupations (n_{D1}, n_{D2}, n_{A1}, n_{A2}) (see Figure 6) that we denote

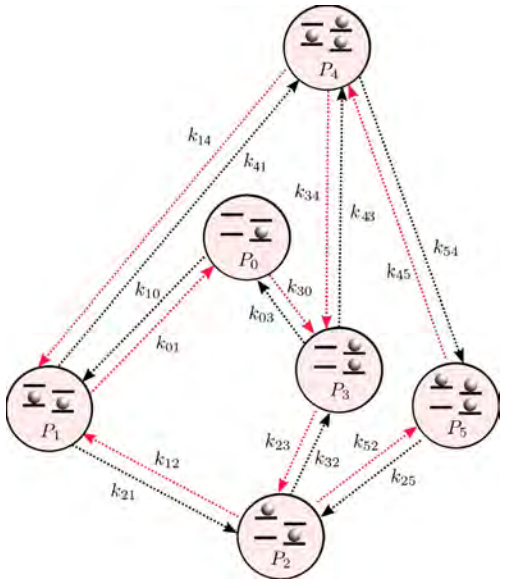

Figure 6. Network representation of the underlying master equation associated with the six accessible microstates. The graph is composed of six vertices (shown as circles). The interconnected vertices represent the probabilities P_N to find the system in a microstate N (N = 0, ..., 5), and the edges connecting some pairs of vertices stand for transitions between the states. The edges are drawn as arrows that indicate transitions with rate $k_{N'N} = k_{N'\leftarrow N}$ from a state (vertex) N to N'.

by the integers N = 0, ..., 5. Within this six-state representation, the probability to find the system in state N is denoted by P_N. The system dynamics is modeled by a master equation accounting for the time evolution of the probabilities $P_N(t)$ (N = 0, ..., 5) fulfilling normalization $\sum_N P_N(t) = 1$ at all times (for details, see ref 33). The steady state is evaluated by setting $dP_N(t)/dt = 0$.

In what follows, we assume that the transition rates $k_{N'N} = k_{N'\leftarrow N}$ from state N to state N' obey (local) detailed balance conditions determined by specified (see below) local temperatures; i.e., their ratios are given by $k_{N'N}/k_{NN'} = \exp(-\beta_\nu \Delta E_{N'N})$, where $\Delta E_{N'N} = E_{N'} - E_N$. Note that in general $\Delta E_{N'N}$ is determined by intrinsic energy differences as well as external driving forces.[68] $\beta_\nu = 1/k_B T_\nu$ is the inverse thermal energy associated with a thermal bath at temperature T_ν. As in the two-level example addressed in Section 2, some of the rate processes are governed by the ambient temperature T, while others reflect external driving force. In the present model the latter are the $1 \leftrightarrow 2$ and $4 \leftrightarrow 5$ transitions, which are governed by the effective temperature T_{eff} defined below.

dx.doi.org/10.1021/jp5084373 | J. Phys. Chem. C 2014, 118, 27226−27234

Because the heterojunction architecture entails an intrinsic energy loss associated with the exciton dissociation, the energetics is determined by both the interfacial gap energy $\Delta\varepsilon$ and the exciton binding energy which is denoted V_c. To understand the role of V_c in the kinetic scheme it is convenient to define it as the energy difference between the energy needed to generate a local exciton (electron in the lowest unoccupied level and hole in the highest occupied level of the same molecule) and the energy of an excitation that places the electron on the LUMO of a neighboring identical molecule. We further assume for simplicity that this exciton binding energy is fully realized at the nearest-neighbor level and does not extend beyond the nearest-neighbor distance. Under this assumption V_c is a property only of the transition between states 2 and 3 (Figure 6) and does not enter into the other transition energies that are calculated from the differences between the corresponding single electron energies ε_{Kj}, K = D,A, j = 1,2. Thus, $E_3 - E_2 = \varepsilon_{A2} - \varepsilon_{D2} + V_c$; however (for example), $E_1 - E_0 = E_4 - E_3 = \varepsilon_{D1} - \mu_L$ and $E_3 - E_0 = E_5 - E_2 = \varepsilon_{A2} - \mu_R$ do not depend on V_c.[78]

With this understanding, the energy differences $\Delta E_{NN'}$ between any two molecular states depicted in Figure 6 can be written and used as described below.

4. THERMODYNAMIC EFFICIENCY LIMIT FROM CYCLE REPRESENTATIONS

The six system states shown in Figure 6 are connected by rate processes, forming a graph in which the states are represented by nodes, while the rate processes correspond to the links between them. This graph can be decomposed into cycles, as detailed in Table 1.

Table 1. Cycles Associated with the Network of the Systems States Given in Figure 6

cycle	path
C_1	$P_0 \to P_1 \to P_2 \to P_3 \to P_0$
C_2	$P_0 \to P_1 \to P_4 \to P_5 \to P_2 \to P_3 \to P_0$
C_3	$P_1 \to P_2 \to P_3 \to P_4 \to P_1$
C_4	$P_2 \to P_3 \to P_4 \to P_5 \to P_2$
C_5	$P_1 \to P_2 \to P_5 \to P_4 \to P_1$
C_6	$P_0 \to P_1 \to P_4 \to P_3 \to P_0$

Let us focus on the fundamental cycle associated with the path C_1: $P_0 \to P_1 \to P_2 \to P_3 \to P_0$. This cycle represents the photovoltaic operation of the considered minimal model for a BHJ-OPV solar cell. In the "forward direction" it starts with electron transfer from the left electrode into level D1 ($P_0 \to P_1$), followed by light-induced promotion of the electron to level D2 ($P_1 \to P_2$), exciton dissociation, that is electron transfer from D2 to A2 ($P_2 \to P_3$), and, finally, transfer of the excess electron on level A2 of the acceptor to the right electrode. These processes are of course accompanied by their reverse counterparts. The energies associated with these transitions are $\Delta E_{10} = \varepsilon_{D1} - \mu_L$, $\Delta E_{21} = \varepsilon_{D2} - \varepsilon_{D1} = \Delta E_D$, $\Delta E_{32} = \varepsilon_{A2} - \varepsilon_{D2} + V_c = V_c - \Delta\varepsilon$, and $\Delta E_{03} = \mu_R - \varepsilon_{A2}$. The corresponding rates satisfy detailed balance conditions that are determined by these energies and the corresponding temperatures. The processes $0 \leftrightarrow 1$, $2 \leftrightarrow 3$, and $3 \leftrightarrow 0$ are governed by the ambient temperature T, that is

$$\frac{k_{10}}{k_{01}} = e^{-(\varepsilon_{D1}-\mu_L)/k_BT} \tag{23}$$

$$\frac{k_{32}}{k_{23}} = e^{-(V_c-\Delta\varepsilon)/k_BT} \tag{24}$$

$$\frac{k_{03}}{k_{30}} = e^{-(\mu_R-\varepsilon_{A2})/k_BT} \tag{25}$$

Consider now the photoinduced $1 \leftrightarrow 2$ process. In general, both the forward and reverse transitions are associated with radiative and nonradiative excitation and recombination that satisfy eqs 19 and 20. Consequently, effective temperature can be defined as in eq 21, where the effective temperature T_{eff} is defined by

$$T_{eff} = \frac{\Delta E_D}{k_B}\frac{1}{\ln\left(\frac{k_{12}^R + k_{12}^{NR}}{k_{21}^R + k_{21}^{NR}}\right)} \tag{26}$$

In the absence of radiationless loss ($k_{12}^{NR} = k_{21}^{NR} = 0$) $T_{eff} = T_S$. In the presence of such loss, eq 26 implies that (since $T < T_S$) $T_{eff} < T_S$. Note that the absolute magnitude of T_{eff} is determined not only by the temperatures T and T_{eff} but also by the kinetic rates themselves: faster nonradiative recombination implies lower effective temperature. Next, suppose that the cycle C_1 represents the entire energy conversion device. Consider the ratio of products of forward and backward, rates, $k_{10}k_{21}k_{32}k_{03}$ and $k_{01}k_{12}k_{23}k_{30}$ in cycle C_1. From eqs 23−25 and 21 we get

$$\frac{k_{10}k_{21}k_{32}k_{03}}{k_{01}k_{12}k_{23}k_{30}} = e^{-(\Delta\mu-\Delta E_D+V_c)/k_BT}e^{-\Delta E_D/k_BT_{eff}} \equiv e^{-A(C_1)/k_BT} \tag{27}$$

where $\Delta\mu = \mu_R - \mu_L$. The quantity $A(C_1)$ defined by eq 27 is the *affinity* of the cycle C_1. It can be recast in the form

$$A(C_1) = \frac{\Delta\mu + V_c - \Delta E_D\eta_{eff}^C}{k_BT} \tag{28}$$

where

$$\eta_{eff}^C = 1 - T/T_{eff} \tag{29}$$

is the Carno efficiency of a reversible machine operating between temperatures T and T_{eff}.

As discussed in Section 2, the cycle affinity vanishes when the cycle carries no current. In this reversible case eq 28 yields

$$\frac{\Delta\mu^{OC}}{\Delta E_D} = \eta_{eff}^C - \frac{V_c}{\Delta E_D} \tag{30}$$

As in eq 6, the left-hand side of this equation represents the energy conversion efficiency of our device. (Note however that efficiency is defined by eq 17 and not according to eq 22.) When $T_{eff} = T_S$ (i.e., in the absence of nonradiative recombination) and $V_c = 0$ (vanishing exciton binding energy), this device operates, in this open-circuit limit, at the Carnot efficiency associated with the sun temperature. Equation 30 shows explicitly the two sources of efficiency reduction in this reversible (open-circuit voltage) situation: the presence of nonradiative recombination which renders an effective temperature lower than T_S and the exciton binding energy that needs to be overcome during the operation at the cost of useful work.

The result (30) is an expression for the maximal efficency of a device operating along cycle C_1. However, it is easily checked that the same condition for vanishing affinity is abtained for any of the cycles in Table 1 that contain the exciton dissociation ($2 \leftrightarrow 3$) step, namely, cycles C_1, C_2, C_3, and C_4. (To verify this

dx.doi.org/10.1021/jp5084373 | J. Phys. Chem. C 2014, 118, 27226−27234

note that $k_{43}/k_{34} = k_{10}/k_{01}$ and $k_{14}/k_{41} = k_{25}/k_{52} = k_{03}/k_{30}$). Furthermore, for both cycles C_5 and C_6 we find $A(C_5) = A(C_6) = 0$. Therefore, the result (30) is valid for the original six-state system depicted in Figures 5 and 6. Note that in the absence of nonradiative recombination, eq 30 becomes

$$\frac{\Delta\mu^{OC}}{\Delta E_D} = \eta^C - \frac{V_c}{\Delta E_D};\ \eta^C = 1 - T/T_S \tag{31}$$

which is compatible with the result of ref 21.

Focusing again on cycle C_1, it should be noted that while it is indeed a cycle as far as the system is concerned traversing this cycle (as well as some of the other cycles) entails a transfer of electron between two sides of the system. While this has no consequence for the calculation of the open-circuit voltage from the condition that the average current vanishes as done here, it is expressed in the equilibrium limit ($T_{eff} = T$ and $\Delta\mu = 0$) of eq 27 by the fact that the r.h.s. of this equation becomes e^{-V_c/k_BT}. This is the Boltzmann factor associated with the charge separation process. At equilibrium, such charge separation corresponds to a voltage fluctuation of small but finite probability. (In an open system such processes lead to observable current fluctuations in the external part of the circuit.) Such fluctuations are canceled on the average by equally improbable fluctutations in the opposite direction. At the nonequilibrium steady state considered above the same processes lead to average current, and the OC voltage 30 or 31 is obtained from the cycle analysis as the condition for its suppression.

Equations 26, 29, and 30 provide a simple and transparent view of the sources of OC voltage reduction and reversible efficiency loss in BHJ-OPV cells. We have checked this result by solving the underlying master equation given in ref 34. To this end we have adapted the energetics and the transition rates used in this previous work,[34] $\mu_L = 0.0$ eV, $\mu_R = \mu_L + \Delta\mu$, $\varepsilon_{D1} = -0.1$ eV, $\varepsilon_{D2} = 1.4$ eV, $\varepsilon_{A2} = 1.15$ eV, and $V_c = 0.15$ eV, and have set the temperatures to $T = 300$ K and $T_S = 6000$ K so the Carnot efficiency is $\eta_C = 0.95$. For simplicity we neglect radiationless losses on the donor.[81] The numerical calculation gives the open-circuit voltage $\Delta\mu^{OC} = 1.275$ eV, which agrees exactly with that value predicted by eq 31, i.e., $\Delta\mu^{OC} = 0.95\Delta E_D - 0.15$ eV $= 1.275$ eV. For $V_C = 0.15$ eV, the maximal achievable thermodynamic efficiency is $\eta^{th} = 0.85$.

5. CONCLUSION AND PERSPECTIVES

We have presented a novel concept for performance analysis of photovoltaic cells and have applied it to the simplest two-level device model as well as a generic model for an organic photovoltaic cell. The starting point is the modeling of the energy conversion process by a set of kinetic (master) equations with rate coefficients that connect between distinct system states. Such rates incorporate the system energy level structure as well as the relevant energetic, thermal, and optical constraints and driving forces. Further analysis is facilitated by describing the resulting master equation as a graph in which the rates are represented by edges that link between vortices representing states. This makes it possible to exploit the decomposition of the network into cycles to get better insight on the interrelations between the physical fluxes. Such a kinetic scheme can be used to analyze the system performance at and away from equilibrium, as was demonstrated here for two simple models that can be analyzed analytically. In the zero power (open voltage) limit, the simplest subclass of systems are those in which all internal currents, therefore all cycle affinities, vanish. The performance of such systems does not depend on individual rates, only on ratios between backward and forward rates that are determined by detailed balance conditions. For the two-level/three-state device model of refs 30 and 32 this analysis yields the Carnot value for the maximum OC efficiency. This is a simple example of a general result: the open-circiut voltage and the corresponding effciency can be calculated from the affinity associated with a network scheme of the underlying rate processes. A similar calculation for a generic model of a bulk heterojunction organic photovoltaic (BHJ-OPV) cell that incorporates the exciton dissociation energy as well as nonradiative recombination in the donor subsystem leads to a maximum OC efficiency and OC voltage that are lower than the limiting Carnot value. For example, with our choice of (reasonable) parameters the maximum available efficiency is found to be 0.85, which is ∼10% lower than the corresponding Carnot value (∼0.95).

A prerequisite for the network-based approach in the form presented here is the ability to cast the essential system dynamics as a network of (Markovian) rate processes. This is obviously not a trivial task as the systems pertaining to useful photovoltaic devices are often complex and not fully characterized. At the same time, the power and flexibility of network-based kinetic descriptions should motivate an effort to construct such descriptions as useful approximations to the actual relevant system dynamics. Analogy can be drawn from recent developments in equally complex systems, proteins, where it was found useful to cast the long-term dynamics in terms of networks of Markov rate processes.[82−84]

The approach presented in this paper can be generalized in several ways. An analysis of the six-level BHJ-OPV model under finite overall current will yield efficiency at maximum power for this model. Constructing and analyzing more complex network models that account also for hot excitons and nuclear reorganization[85] is an important extension. Even under OC conditions, loss due to the presence of cycles with nonvanishing currents can be encountered in more complex models and should be accounted for. Finally, extending such an approach to the quantum-mechanical regime may be of interest. These will be the subject of future efforts.

■ ASSOCIATED CONTENT

Supporting Information

More details on the calculation that yields the results in Figures 3 and 4. This material is available free of charge via the Internet at http://pubs.acs.org.

■ AUTHOR INFORMATION

Corresponding Authors

*E-mail: meinax@al.tau.ac.il.

*E-mail: nitzan@post.tau.ac.il.

Notes

The authors declare no competing financial interest.

■ ACKNOWLEDGMENTS

The research is supported by the Israel Science Foundation, the Israel-US Binational Science Foundation (grant No. 2011509), and the European Science Council (FP7/ERC grant No. 226628). We thank Mark Ratner, Philip Ruyten and Bart Cleuren for stimulating discussions. A.N. thanks the Chemistry Department at the University of Pennsylvania and the Physics

Department of the Free University of Berlin for hospitality during the time this paper was completed.

REFERENCES

(1) Nelson, J. *The Physics of Solar Cells*; World Scientific: Singapore, 2003.

(2) Würfel, P. *Physics of Solar Cells: From Basic Principles to Advanced Concepts*, 2nd ed.; Wiley VCH: Weinheim, 2009.

(3) Nayak, P.; Garcia-Belmonte, G.; Kahn, A.; Bisquert, J.; Cahen, D. Photovoltaic Efficiency Limits and Material Disorder. *Energy Environ. Sci.* **2012**, *5*, 6022−39.

(4) *Physics of Organic Semiconductors*, 2nd ed.; Brutting, W.; Adachi, C., Eds.; Wiley VCH: Weinheim, 2012.

(5) Dennler, G.; Scharber, M. C.; Brabec, C. J. Polymer-Fullerene Bulk-Heterojunction Solar Cells. *Adv. Mater.* **2009**, *21*, 1323−38.

(6) Chen, H.-Y.; Hou, J.; Zhang, S.; Liang, Y.; Yang, G.; Yang, Y.; Yu, L.; Wu, Y.; Li, G. Polymer Solar Cells with Enhanced Open-Circuit Voltage and Efficiency. *Nat. Photonics* **2009**, *3*, 649−53.

(7) Brédas, J.-L.; Norton, J. E.; Cornil, J.; Coropceanu, V. Molecular Understanding of Organic Solar Cells: The Challenges. *Acc. Chem. Res.* **2009**, *42*, 1691−99.

(8) Deibel, C.; Dyakonov, V. Polymer−Fullerene Bulk Heterojunction Solar Cells. *Rep. Prog. Phys.* **2010**, *73*, 096401.

(9) Nicholson, P. G.; Castro, F. A. Organic Photovoltaics: Principles and Techniques for Nanometre Scale Characterization. *Nanotechnology* **2010**, *21*, 492001.

(10) Thompson, B. C.; Khlyabich, P. P.; Burkhart, B.; Aviles, A. E.; Rudenko, A.; Shultz, G. V.; Ng Christi, F.; Mangubat, L. B. Polymer-Based Solar Cells: State-of-the-Art Principles for the Design of Active Layer Components. *Green* **2011**, *1*, 29−54.

(11) Nelson, J. Polymer:Fullerene Bulk Heterojunction Solar Cells. *Mater. Today* **2011**, *14*, 462−70.

(12) Camaioni, N.; Po, R. Pushing the Envelope of the Intrinsic Limitation of Organic Solar Cells. *J. Phys. Chem. Lett.* **2013**, *4*, 1821−28.

(13) Seki, K.; Furube, A.; Yoshida, Y. Detailed Balance Limit of Power Conversion Efficiency for Organic Photovoltaics. *Appl. Phys. Lett.* **2013**, *103*, 253904.

(14) Potscavage, W. J.; Sharma, A.; Kippelen, B. Critical Interfaces in Organic Solar Cells and Their Influence on the Open-Circuit Voltage. *Acc. Chem. Res.* **2009**, *42*, 1758−67.

(15) Wagenpfahl, A.; Deibel, C.; Dyakonov, V. Organic Solar Cell Efficiencies under the Aspect of Reduced Surface Recombination Velocities. *IEEE J. Sel. Top. Quantum Electron.* **2010**, *16*, 1759−63.

(16) Koster, L. J. A.; Shaheen, S. E.; Hummelen, J. C. Pathways to a New Efficiency Regime for Organic Solar Cells. *Adv. Energy Mater.* **2012**, *2*, 1246−53.

(17) Gruber, M.; Wagner, J.; Klein, K.; Hörmann, U.; Opitz, A.; Stutzmann, M.; Brütting, W. Thermodynamic Efficiency Limit of Molecular Donor-Acceptor Solar Cells and Its Application to Diindenoperylene/C60-Based Planar Heterojunction Devices. *Adv. Energy Mater.* **2012**, *2*, 1100−08.

(18) Shockley, W.; Queisser, H. J. Detailed Balance Limit of Efficiency of P-N Junction Solar Cells. *J. Appl. Phys.* **1961**, *32*, 510−19.

(19) Henry, C. H. Limiting efficiencies of ideal single and multiple energy gap terrestrial solar cells. *J. Appl. Phys.* **1980**, *51*, 4494−4500.

(20) Landsberg, P. T.; Tonge, G. Thermodynamic Energy Conversion Efficiencies. *J. Appl. Phys.* **1980**, *51*, R1−R20.

(21) Giebink, N. C.; Wiederrecht, G. P.; Wasielewski, M. R.; Forrest, S. R. Thermodynamic Efficiency Limit of Excitonic Solar Cells. *Phys. Rev. B* **2011**, *83*, 195326.

(22) Scharber, M. C.; Sariciftci, N. S. Efficiency of Bulk-Heterojunction Organic Solar Cells. *Prog. Polym. Sci.* **2013**, *38*, 1929−40.

(23) Green, M. A. Time-Asymmetric Photovoltaics. *Nano Lett.* **2012**, *12*, 5985−88.

(24) Sylvester-Hvid, K. O.; Rettrup, S.; Ratner, M. A. Two-Dimensional Model for Polymer-Based Photovoltaic Cells: Numerical Simulations of Morphology Effects. *J. Phys. Chem. B* **2004**, *108*, 4296−307.

(25) Rau, U. Reciprocity Relation between Photovoltaic Quantum Efficiency and Electroluminescent Emission of Solar Cells. *Phys. Rev. B* **2007**, *76*, 085303.

(26) Kirchartz, T.; Rau, U. Detailed Balance and Reciprocity in Solar Cells. *Phys. Status Solidi (a)* **2008**, *205*, 2737−51.

(27) Kirchartz, T.; Taretto, K.; Rau, U. Efficiency Limits of Organic Bulk Heterojunction Solar Cells. *J. Phys. Chem. C* **2009**, *113*, 17958−66.

(28) Vandewal, K.; Tvingstedt, K.; Gadisa, A.; Inganas, O.; Manca, J. V. On the Origin of the Open-Circuit Voltage of Polymer-Fullerene Solar Cells. *Nat. Mater.* **2009**, *8*, 904−09.

(29) Miyadera, T.; Wang, Z.; Yamanari, T.; Matsubara, K.; Yoshida, Y. Efficiency Limit Analysis of Organic Solar Cells: Model Simulation Based on Vanadyl Phthalocyanine/C 60 Planar Junction Cell. *Jpn. J. Appl. Phys.* **2014**, *53*, 01AB12.

(30) Nelson, J.; Kirkpatrick, J.; Ravirajan, P. Factors Limiting the Efficiency of Molecular Photovoltaic Devices. *Phys. Rev. B* **2004**, *69*, 035337.

(31) Markvart, T. Solar Cell as a Heat Engine: Energy−Entropy Analysis of Photovoltaic Conversion. *Phys. Status Solidi (a)* **2008**, *205*, 2752−56.

(32) Rutten, B.; Esposito, M.; Cleuren, B. Reaching Optimal Efficiencies Using Nanosized Photoelectric Devices. *Phys. Rev. B* **2009**, *80*, 235122.

(33) Einax, M.; Dierl, M.; Nitzan, A. Heterojunction Organic Photovoltaic Cells as Molecular Heat Engines: A Simple Model for the Performance Analysis. *J. Phys. Chem. C* **2011**, *115*, 21396−401.

(34) Einax, M.; Dierl, M.; Schiff, P. R.; Nitzan, A. Multiple State Representation Scheme for Organic Bulk Heterojunction Solar Cells: A Novel Analysis Perspective. *Europhys. Lett.* **2013**, *104*, 40002.

(35) Wang, H.; Wu, G. X. Performance Analysis and Optimum Criteria of a Quantum Dot Engine with Two Discrete Energy Levels. *Phys. Lett. A* **2012**, *376*, 2209−16.

(36) Scully, M. O. Quantum Photocell: Using Quantum Coherence to Reduce Radiative Recombination and Increase Efficiency. *Phys. Rev. Lett.* **2010**, *104*, 207701.

(37) Kirk, A. P. Analysis of Quantum Coherent Semiconductor Quantum Dot P-I-N Junction Photovoltaic Cells. *Phys. Rev. Lett.* **2011**, *106*, 048703.

(38) Scully, M. O. Comment on "Analysis of Quantum Coherent Semiconductor Quantum Dot P-I-N Junction Photovoltaic Cells". *Phys. Rev. Lett.* **2011**, *106*, 049801.

(39) Goswami, H. P.; Harbola, U. Thermodynamics of Quantum Heat Engines. *Phys. Rev. A* **2013**, *88*, 013842.

(40) The separation between 'internal' and 'external' factors can depend on the system considered or rather on the model used to describe it. For example, following SQ,[18] it is often assumed that all radiation absorbed by the system quickly finds its way to the lowest electronically excited state. The associated loss then can be cast as part of the 'external' contribution to the overall efficiency. If the dynamics of this process is considered important (with possible contribution of hot excitons to the charge separation process), the contribution of processes undergone by the relevant excited states needs to be taken as part of the internal efficiency. This will result in a more complex network of states and rates that can be treated within the approach presented in this paper.

(41) Andresen, B. Current Trends in Finite-Time Thermodynamics. *Angew. Chem., Int. Ed.* **2011**, *50*, 2690−704.

(42) Agrawal, D. C. A Finite Speed Curzon-Ahlborn Engine. *Eur. J. Phys.* **2009**, *30*, 587−92.

(43) Esposito, M.; Lindenberg, K.; Van den Broeck, C. Universality of Efficiency at Maximum Power. *Phys. Rev. Lett.* **2009**, *102*, 130602−4.

(44) Esposito, M.; Kawai, R.; Lindenberg, K.; Van den Broeck, C. Efficiency at Maximum Power of Low-Dissipation Carnot Engines. *Phys. Rev. Lett.* **2010**, *105*, 150603.

(45) Abe, S. Maximum-Power Quantum-Mechanical Carnot Engine. *Phys. Rev. E* **2011**, *83*, 041117.
(46) Apertet, Y.; Ouerdane, H.; Goupil, C.; Lecoeur, P. Efficiency at Maximum Power of Thermally Coupled Heat Engines. *Phys. Rev. E* **2012**, *85*, 041144.
(47) Moreau, M.; Gaveau, B.; Schulman, L. S. Efficiency of a Thermodynamic Motor at Maximum Power. *Phys. Rev. E* **2012**, *85*, 021129.
(48) Van den Broeck, C.; Kumar, N.; Lindenberg, K. Efficiency of Isothermal Molecular Machines at Maximum Power. *Phys. Rev. Lett.* **2012**, *108*, 210602.
(49) Van den Broeck, C.; Lindenberg, K. Efficiency at Maximum Power for Classical Particle Transport. *Phys. Rev. E* **2012**, *86*, 041144.
(50) Wang, J.; He, J.; Wu, Z. Efficiency at Maximum Power Output of Quantum Heat Engines under Finite-Time Operation. *Phys. Rev. E* **2012**, *85*, 031145.
(51) Wang, Y.; Tu, Z. C. Efficiency at Maximum Power Output of Linear Irreversible Carnot-Like Heat Engines. *Phys. Rev. E* **2012**, *85*, 011127.
(52) Allahverdyan, A. E.; Hovhannisyan, K. V.; Melkikh, A. V.; Gevorkian, S. G. Carnot Cycle at Finite Power: Attainability of Maximal Efficiency. *Phys. Rev. Lett.* **2013**, *111*, 050601.
(53) Gonzalez-Ayala, J.; Arias-Hernandez, L. A.; Angulo-Brown, F. Connection between Maximum-Work and Maximum-Power Thermal Cycles. *Phys. Rev. E* **2013**, *88*, 052142.
(54) Hooyberghs, H.; Cleuren, B.; Salazar, A.; Indekeu, J. O.; Van den Broeck, C. Efficiency at Maximum Power of a Chemical Engine. *J. Chem. Phys.* **2013**, *139*, 134111.
(55) Wang, R.; Wang, J.; He, J.; Ma, Y. Efficiency at Maximum Power of a Heat Engine Working with a Two-Level Atomic System. *Phys. Rev. E* **2013**, *87*, 042119.
(56) Izumida, Y.; Okuda, K. Work Output and Efficiency at Maximum Power of Linear Irreversible Heat Engines Operating with a Finite-Sized Heat Source. *Phys. Rev. Lett.* **2014**, *112*, 180603.
(57) Roßnagel, J.; Abah, O.; Schmidt-Kaler, F.; Singer, K.; Lutz, E. Nanoscale Heat Engine Beyond the Carnot Limit. *Phys. Rev. Lett.* **2014**, *112*, 030602.
(58) Hill, T. L. Studies in Irreversible Thermodynamics Iv. Diagrammatic Representation of Steady State Fluxes for Unimolecular Systems. *J. Theor. Biol.* **1966**, *10*, 442−59.
(59) Schnakenberg, J. Network Theory of Microscopic and Macroscopic Behavior of Master Equation Systems. *Rev. Mod. Phys.* **1976**, *48*, 571−85.
(60) Zia, R. K. P.; Schmittmann, B. Probability Currents as Principal Characteristics in the Statistical Mechanics of Non-Equilibrium Steady States. *J. Stat. Mech.* **2007**, *2007*, P07012.
(61) Andrieux, D.; Gaspard, P. Fluctuation Theorem for Currents and Schnakenberg Network Theory. *J. Stat. Phys.* **2007**, *127*, 107−31.
(62) Gaspard, P. In *Nonlinear Dynamics of Nanosystems*; Radons, G., Rumpf, B., Schuster, H. G., Eds.; Wiley-VCH: Weinheim, 2010; pp 1−74.
(63) Altaner, B.; Grosskinsky, S.; Herminghaus, S.; Katthän, L.; Timme, M.; Vollmer, J. Network Representations of Nonequilibrium Steady States: Cycle Decompositions, Symmetries, and Dominant Paths. *Phys. Rev. E* **2012**, *85*, 041133.
(64) Seifert, U. Stochastic Thermodynamics, Fluctuation Theorems and Molecular Machines. *Rep. Prog. Phys.* **2012**, *75*, 126001.
(65) Kirchhoff, G. *Ann. Phys. (Berlin)* **1847**, *148*, 497.
(66) Andrieux, D.; Gaspard, P. Fluctuation Theorem and Onsager Reciprocity Relations. *J. Chem. Phys.* **2004**, *121*, 6167−74.
(67) GASPARD, P.; GERRITSMA, E. Chemomechanical Coupling and Stochastic Thermodynamics of the F1-Atpase Molecular Motor with an Applied External Torque. *Biophys. Rev. Lett.* **2010**, *05*, 163−208.
(68) Einax, M.; Solomon, G.; Dieterich, W.; Nitzan, A. Unidirectional Hopping Transport of Interacting Particles on a Finite Chain. *J. Chem. Phys.* **2010**, *133*, 054102.
(69) Einax, M.; Körner, M.; Maass, P.; Nitzan, A. Nonlinear Hopping Transport in Ring Systems and Open Channels. *Phys. Chem. Chem. Phys.* **2010**, *12*, 645−54.
(70) Dierl, M.; Maass, P.; Einax, M. Time-Dependent Density Functional Theory for Driven Lattice Gas Systems with Interactions. *Condens. Matter: Stat. Mech.* **2011**, *93*, 50003.
(71) Dierl, M.; Maass, P.; Einax, M. Classical Driven Transport in Open Systems with Particle Interactions and General Couplings to Reservoirs. *Phys. Rev. Lett.* **2012**, *108*, 060623.
(72) Burlakov, V. M.; Kawata, K.; Assender, H. E.; Briggs, G. A. D.; Ruseckas, A.; Samuel, I. D. W. Discrete Hopping Model of Exciton Transport in Disordered Media. *Phys. Rev. B* **2005**, *72*, 075206.
(73) Rühle, V.; Lukyanov, A.; May, F.; Schrader, M.; Vehoff, T.; Kirkpatrick, J.; Baumeier, B.; Andrienko, D. Microscopic Simulations of Charge Transport in Disordered Organic Semiconductors. *J. Chem. Theory Comput.* **2011**, *7*, 3335−45.
(74) Baruch, P. A Two-Level System as a Model for a Photovoltaic Solar Cell. *J. Appl. Phys.* **1985**, *57*, 1347−55.
(75) Obviously, as long as the pumping and relaxation are represented by kinetic rates, an effective temperature can be defined. It is often referred to as "sun temperature"; however, it is usually a more complex quantity as some of the processes that cause transition between states 1 and 2, for example, nonradiative relaxation (i.e., recombination), are associated with the ambient environment, see eq 12.
(76) Curzon, F. L.; Ahlborn, B. Efficiency of a Carnot Engine at Maximum Power Output. *Am. J. Phys.* **1975**, *43*, 22−24.
(77) Because level A1 is restricted to be always occupied, the single electron energy εA2 is taken to include the Coulombic repulsion between two electrons on the acceptor. This notation is different from that of refs 33 and 34, where we have referred to this repulsive interaction explicitly
(78) Physically, the exciton binding energy represents the fact that the process 2 ⇌ 3 generates a voltage drop within the system, and the exciton binding energy is the energy needed to generate this drop. It is of course also possible to assign the exciton binding energy to the individual states in our model as recently argued by Zhu.[79] In this case all states in which charge separation has been realized will be shifted in energy by this voltage drop, V_o, from all states in which it was not, and the ensuing rates will be the same as outlined below. The assumption (made for simplicity) that the exciton binding energy is fully realized at the nearest neighbor level can be restated as an assumption that this voltage drop is localized at the position where exciton dissociation occurs, namely, at the donor−acceptor interface. This voltage drop is experimentally observed[80] although in reality it can spread over a somewhat larger distance
(79) Zhu, X. Y. How to Draw Energy Level Diagrams in Excitonic Solar Cells. *J. Phys. Chem. Lett.* **2014**, *5*, 2283−88.
(80) Jailaubekov, A. E.; Willard, A. P.; Tritsch, J. R.; Chan, W.-L.; Sai, N.; Gearba, R.; Kaake, L. G.; Williams, K. J.; Leung, K.; Rossky, P. J.; Zhu, X. Y. Hot Charge-Transfer Excitons Set the Time Limit for Charge Separation at Donor/Acceptor Interfaces in Organic Photovoltaics. *Nat. Mater.* **2013**, *12*, 66−73.
(81) In this case the maximum achievable efficiency value for the chosen parameter set depends only on the detailed balance ratio and is not affected by the specific form of the transition rates for the electron hopping between the reservoirs and the molecule sites as well as between the donor and acceptor molecules.
(82) Chennubhotla, C.; Bahar, I. Markov Methods for Hierarchical Coarse-Graining of Large Protein Dynamics. *J. Comput. Biol.* **2007**, *14*, 765−76.
(83) Glowacki, D. R.; Harvey, J. N.; Mulholland, A. J. Taking Ockham's Razor to Enzyme Dynamics and Catalysis. *Nat. Chem.* **2012**, *4*, 169−76.
(84) Kreuzer, S. M.; Elber, R.; Moon, T. J. Early Events in Helix Unfolding under External Forces: A Milestoning Analysis. *J. Phys. Chem. B* **2012**, *116*, 8662−91.
(85) The effect of nuclear reorganization has recently been discussed by us using another approach.[34]